Medical Diagnostic System Based On Simultaneous Multispectral Fluorescence Imaging

Andersson-Engels, Stefan; Johansson, Jonas; Svanberg, Sune

Published in:
Applied Optics

DOI:
10.1364/AO.33.008022

1994

Medical diagnostic system based on simultaneous multispectral fluorescence imaging

Stefan Andersson-Engels, Jonas Johansson, and Sune Svanberg

A multicolor fluorescence imaging system applied to medical diagnostics is described. The system presented simultaneously records four fluorescence images in different wavelength bands, permitting low-resolution spectroscopy imaging. An arithmetic function image of the four spectral images is constructed by a pixel-to-pixel calculation and is presented on a monitor in false-color coding. A sensitive detector is required for minimizing the excitation energy necessary to obtain an image and thus avoid side effects on the investigated tissue. Characteristics of the system of importance for the detector sensitivity as well as image quality are discussed. A high degree of suppression of ambient background light is reached with this system by the use of a pulsed laser as an excitation source together with gated detection. Examples of fluorescence images from tumors on the hind legs and in the brain of rats injected with Photofrin are given.

Key words: Tissue diagnostics, fluorescence, imaging, spectroscopy, hematoporphyrin, cancer.

1. Introduction

Diagnostic techniques for early localization of diseased tissue are of great medical interest. New techniques, which are complementary diagnostic alternatives to existing methods, are under development. Among these techniques, optical spectroscopy has shown a promising potential.[1–6] Diffuse reflection, transmittance, and fluorescence spectroscopy seem particularly interesting for *in vivo* diagnostic use. All are sensitive techniques, limiting the necessary light dose to be delivered to the tissue. Diffuse reflection and transmittance spectroscopy can be used to probe the concentration of a major chromophore in a tissue volume, whereas fluorescence spectroscopy has been utilized mostly for superficial measurements to be able to distinguish between different tissue types. Quantitative measurements of tissue fluorophores may yield limited accuracy, as their fluorescence yield is often sensitive to the microenvironment of the fluorophore.[7] Varying results could thus be explained by a difference in localization rather than by concentration of the fluorophore. However, promising results have been shown in the field of early detection and localization of malignant tumors.[1,2] The detection is most often based on the characteristic fluorescence signature of an administered porphyrin derivative as a marker for malignant tissue. Photofrin (Quadra Logics Inc., Vancouver), still the most widely used fluorescent tumor marker, is developed as a photosensitizer for photodynamic therapy (PDT) and is selectively retained in malignant tumors. Now several other second-generation drugs with improved characteristics for PDT and fluorescence tumor marking are being tested in clinical trials. The photophysical mechanisms used are the same for all the drugs under development. On excitation several deexcitation processes are possible. A transition from the excited singlet state to the first excited triplet state is the first step in the photodynamic process of PDT that yields tissue oxidation, whereas a direct deexcitation under emission of light to the ground state results in fluorescence. Most fluorescent tumor-marking drugs yield a characteristic dual-peaked fluorescence in the red spectral region, which may be utilized for diagnostics of malignant tumors.

Several different types of diagnostic instrumentation, making use of the characteristic tumor-marker fluorescence, have been developed.[8] The aim with these systems has been to discriminate directly between malignant and healthy tissue in situations in which this is not possible with other techniques. The main differences between the various equipments are to be found in complexity, processing, and presentation. Imaging, as well as point monitoring,

The authors are with the Department of Physics, Lund Institute of Technology, P.O. Box 118, S-221 00 Lund, Sweden.

Received 3 January 1994; revised manuscript received 13 May 1994.

0003-6935/94/348022-08$06.00/0.

instrumentations have been described. Also the spectral coverage has varied from a single-wavelength band to the entire fluorescence spectrum. Low-resolution tissue spectroscopy is often satisfactory, as tissue fluorescence by nature is smooth and unstructured, and only a few wavelengths may be adequate for obtaining all useful information in the tissue fluorescence spectrum. To detect more than one wavelength is, however, of importance, to permit the tissue autofluorescence to be subtracted from the porphyrin fluorescence and in this way increase the contrast between diseased and nondiseased tissue. To overcome the limitation with a single-wavelength imaging system, a few imaging systems that use a dual-camera system or with sequential recordings of two different fluorescence intensities have been developed.[9–13] Furthermore, it has been shown that tissue autofluorescence can provide a contrast between tumorous and nontumorous regions.[14–16] By forming a ratio between the pure tumor-making drug fluorescence and the tissue autofluorescence, one can take advantage of a dimensionless quantity with an enhanced contrast between tumorous and nontumorous regions compared with measurements of the drug fluorescence only.

This paper presents the characteristics of a multicolor fluorescence imaging system with simultaneous recordings of four different fluorescence images developed following the ideas outlined in earlier papers.[17,18] The principle is based on a split-mirror optical system that forms four identical images of the object in the four quadrants of a rectangular imaging detector. Each image can then be filtered individually by bandpass filters for the fluorescence wavelengths of interest. After the four subimages are read out to a computer, an artificial image can be calculated from the intensity values in pixels of the four subimages that correspond to the same location in the object and in this way form a function image pixel by pixel. Because the fluorescence intensities at four different wavelengths can be measured, both subtraction of tissue autofluorescence from the tumor-marking drug signal as well as a formation of a dimensionless ratio between the drug fluorescence and the tissue autofluorescence can be used. The main advantage of such a simultaneous measurement instead of sequential measurements is that exactly the same area is imaged in the different fluorescence bands independently of sample movements.

The aim with this project was to develop a system that, with low excitation energy, can differentiate between tissue types in a time scale as close to real time as possible and under a typical background-light level for the appropriate medical examination. First the instrumental arrangement is described. The specifications of the system, with special emphasis on the intensity and the spatial resolution, are discussed. A few examples of images obtained with the equipment are also given. Finally, a discussion of possible improvements and simplifications of the system in certain cases is presented.

2. Material and Methods

A. Detector System

A PRA LN250 sealed-off nitrogen laser that emitted 4-ns-long pulses at 337 nm with a pulse energy of 180 μJ and at a repetition rate of maximum 20 Hz was used as an excitation source. The output beam had the dimension of 12 mm × 4 mm at the laser and a 3-mrad divergence in the x direction and 1 mrad in the y direction.

The optical arrangement used is shown in Fig. 1. The laser beam was focused with quartz cylindrical lenses. The beam was reflected in a dichroic mirror that reflected the laser light and transmitted fluorescent light above 370 nm. At the image plane of the cylindrical lens, the beam size was approximately 10 mm × 10 mm. This plane was defined as the sample plane by a nonfluorescent quartz plate. Further, a nonfluorescent, thin copper mask was placed in between the quartz and the tissue sample under investigation. The 10 mm × 10 mm square-shaped mask defined the sample area. It permitted the sample to be relatively evenly irradiated, while a sharp edge to a nonfluorescent surrounding was of importance to avoid an overlap of the four images detected side by side on the CCD detector.

The tissue fluorescence following the laser excitation was collected with a specially developed Cassegrainian type of telescope. The telescope consists of a filter cassette for four 50 mm × 50 mm bandpass filters, a primary mirror split in four segments, all individually adjustable, and an output mirror. Each of the segments of the primary mirror produced one image of the object. When the segments were tilted individually at an angle of a few degrees from the optical axis, the four identical images were placed one in each quadrant of the rectangular imaging detector surface. The use of different bandpass filters in front of the four primary mirror segments permitted the object to be imaged simultaneously in four different wavelength regions on the same detector. In the

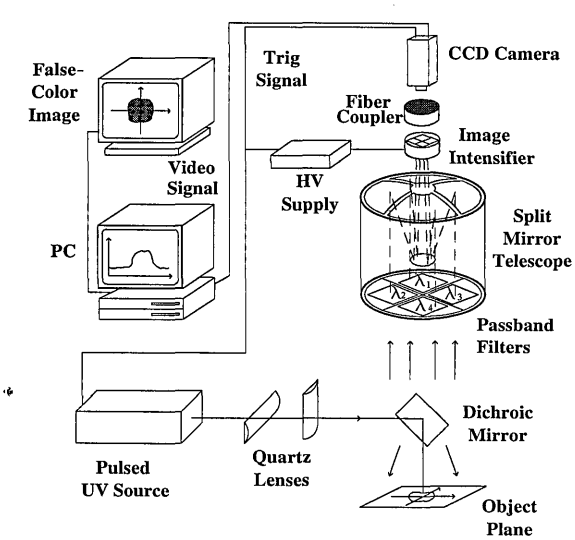

Fig. 1. Setup of the multicolor fluorescence imaging system.

examples shown below, interference filters with a full-width at half-maximum of 10 nm were used. To adjust the brightness of the four images separately and thus utilize the limited dynamic range of the detector optimally, we could vary the actual aperture of the various telescope segments at the filter cassette. The individual adjustments were important in ensuring that the four images had similar brightness. The primary mirror had an outer diameter of 125 mm, an inner diameter of 40 mm, and a radius of curvature of 220 mm. The output mirror had a diameter of 50 mm with a curvature of −280 mm. It was placed 60–110 mm in front of the primary mirror. Both mirrors had a first-surface reflecting layer of aluminum. After initial testing, an aperture was placed in front of the first mirror to reduce the aperture to approximately two thirds of the full telescope aperture and to utilize only central beams. In this way the image resolution was improved with only a small reduction of the signal levels.

A Delli Delti Model CPI/NS2 (modified) dual microchannel plate (MCP) image-intensified CCD camera was used as a detector. In the measurements the camera was used with either one or two MCP's. The first of the two 18-mm-diameter MCP intensifiers had a photocathode with a S20ER response. The intensifier was gatable, with gate widths from 5 ns to 200 μs in length, or it could be run in continuous wave (cw). Normally a 200-ns-long gate width was used in the recordings, for a time long enough to integrate all fluorescent light emitted from the sample while short enough to suppress ambient background light. The phosphors of the MCP intensifiers were of the P20 type. The phosphorescence emission was long lived and ~10% remained after 0.5 ms. The gain of the first MCP intensifier was adjustable up to 2000 times and was almost always used at maximum gain. The second MCP was equipped with an S20 responding photocathode. When used, the gate width of the second MCP was always set to be the longest possible (200 μs) in order to match the phosphorescence lifetime of the P20 phosphor of the first intensifier. The gain of the second intensifier was varied and set so that the signal would match the sensitivity of the CCD camera. The CCD camera was fiber optically coupled to the image intensifiers. The camera was Peltier cooled to ~5 °C to reduce dark current in the camera, which adds to the signal as a background. With the same motivation the integration time of the signal on the CCD chip was reduced to ~2 ms. Longer integration times will only result in a higher background level added to the signal. The signal was subsequently read out to an 8-bit Data Translation frame grabber (Model DT 2851) in an IBM PC-386 compatible computer with the standard CCIR video format, matching the dynamics of the signals coming from the camera. The analog-to-digital converted data were fed to an extra numerical array processor (Data Translation Model DT7020) in order to pinpoint the calculation speed of the subsequent image processing.

B. Recording Procedure

To start the image acquisition, the system waits for the CCD camera to give an image synchronization signal. This signal is fed to the computer, and the computer sends trigger signals to the laser and the image intensifier electronics. The laser fires, and the image intensifiers are simultaneously gated to integrate the fluorescence. The output of the image intensifiers is recorded by the CCD camera. The image is then read out as a CCIR video signal to the frame grabber in the computer. After the analog-to-digital conversion and the data transfer to the array processor, the cycle can restart. Data recording and processing of prior images can work in parallel, as the array processor can work independently of the host processor.

The computer processing is based on software written in standard FORTRAN'77 utilizing libraries with subroutines for the frame grabber and array processor supplied with these items. The image acquisition and processing program includes several accumulation modes, with different averaging and time constants. Normally, averaging of 10 to 50 readouts is necessary to obtain good-quality images. However, for adjustments (of optics or intensifier gain), each recording can be presented unprocessed and updated at 8 Hz. Furthermore, the image should be corrected for dark-current signals and sensitivity at different locations in the image. To correct for dark-current signals, it is necessary to record an image with a dark-current signal only and subtract this image from any data image. The dark current may change during longer periods of data collection, and dark-current images should therefore be recorded repeatedly during a series of experiments. Variation in the system sensitivity over an image can be due to either a noneven distribution of the excitation light over the object or to spatial variations in the detection sensitivity. Almost all such effects will be taken care of by multicolor processing, meaning that such a correction is useful only when the unprocessed images are to be studied. To correct for variations in spatial sensitivity, fluorescence images for a nonstructured object with even fluorescence characteristics over the entire surface can be recorded. The first images presented in this paper are corrected with fluorescence images obtained from a cuvette filled with heavy fuel oil. Heavy fuel oil was chosen, as the excitation light penetrates only a few micrometers into the oil, resulting in a sharply defined image plane. Furthermore, the broad fluorescence emission of heavy oil from ~400 to 750 nm permits spatial correction at all detection wavelengths as well as spectral correction for the detector sensitivity at the various wavelengths. In other examples the true raw data images are presented together with the processed image.

C. Imaging Samples

Two rat tumor models were examined with the system, one colon adenocarcinoma inoculated in the hind legs of Wistar–Furth rats and one glioma inocu-

lated in the brain of Fischer-344 rats. The adenocarcinoma-bearing rats were prepared as described in Ref. 14. Briefly, the tumors were ~2 mm in diameter at the time of the investigation. Two days before the fluorescence examination, 5 mg/kg body weight of Photofrin was injected intravenously. The animals were sacrificed just before the examination. The skin was then carefully removed, and the tumor and surrounding muscle were exposed for the fluorescence imaging system. Visual inspection was sufficient to determine the size of the tumors.

The experimental preparation procedure for the RG-2 tumor followed the description given in Ref. 19. The animal was injected intravenously with 1 mg/kg body weight with Photofrin on day 16 after glioma cell inoculation in the right hemisphere of the rat brain. The animal was sacrificed 24 h later. The brain was then removed from the skull and was investigated by the fluorescence imaging system. The tumor size was determined by visual inspection.

D. System Performance Tests

The background signal without fluorescent light was recorded by blocking out the excitation laser light. The nonsignal-related noise was measured when two such images were subtracted from each other and the standard deviation of the individual pixel values was taken from their mean value.

The system sensitivity was measured with one and two MCP's. The fluorescence from an ethanol solution of Rhodamine 6G filtered through Schott color glass filter GG420 was measured and the rhodamin concentration, for which the signal-to-noise ratio was unity, was found. The solution was contained in a 10-mm-thick quartz cuvette.

The linearity of the detection was measured at various gains by recording the fluorescence signal from Rhodamine 6G (Rh6G) in a ethanol solution filtered through Schott color glass filter GG420 and various neutral-density filters. In similar measurements the dynamic range (the ratio between the highest and the lowest signal detectable) was obtained.

Finally, the spatial resolution of the system (which is defined as how many line pairs could be resolved with the system) was investigated. This is best described by the system modulation transfer function (MTF). The spatial resolution of the system was obtained by fluorescence recordings of a test image. The imaged object was composed of a bright fluorescent paper striped with nonfluorescent metallic bands with varying spatial periods. Preliminary measurements showed that the resolution was limited by the optics rather than by the camera.

3. Results

A. System Characteristics

When the camera was cooled with a Peltier element, the dark-current level of the CCD camera was below one count for one readout on the 255-level analog-to-digital conversion. The dark signal noise was thus no limitation, yielding the lowest detectable signal of one count, and the dynamic range for one MCP was in excess of 100 for a single readout. When two MCP's were used, the system was photon counting and the dynamic range was limited by the number of counts that one photon represents. At full gain on both MCP's, one photon will saturate the camera, yielding a dynamic range of only unity. In the measurements with two MCP's, we never applied more than half the maximum voltage over the MCP's, which yielded a dynamic range of approximately 15 for one readout. The sensitivity was ~1 part in 10^9 (ppb) Rh6G in the 1-cm cuvette for two MCP's, corresponding to one detected photon/pixel of the intensified CCD camera and better than 30 ppb for a single MCP. As the signal-to-noise ratio improves with the number of accumulated readouts, both the dynamic range and the sensitivity will improve with accumulation.

The linearity was measured for both high and low gains for one MCP. The results are shown in Fig. 2. Averaging of 200 readouts was used to avoid fluctuations caused by gain variations in the MCP. The curves show a near-linear response with only a slight deviation at high light intensities.

The plot of the MTF of the entire system obtained with a striped test object is shown in Fig. 3 as a function of line-pair separation. During all measurements presented in this paper an aperture was used in front of the first mirror in the telescope to shield the outer parts of the mirror. In this way the resolution was improved, with only a minor reduction in the signal levels. The system with this aperture was able to resolve line pairs with a spatial period in the object of 2 mm^{-1} with a MTF of 0.2, corresponding to ~70 line pairs over the entire CCD array.

B. Measurement Examples

In Figs. 4 and 5 the results from three Photofrin-marked rodent tumors, imaged with the system with one MCP, are presented. The examples show, in the tumor region, high porphyrin signals at 630 nm and a decrease in the blue–green tissue autofluorescence at 470 nm, as is normally seen from tumors. In Fig. 4, the three images at 630, 600, and 470 nm are shown. The images show the same area (10 mm × 10 mm) of a rat muscle. At 1:00 p.m. in the images a 1.5 mm × 3 mm inoculated adenocarcinoma tumor is present. These images are corrected for nonuniform illumina-

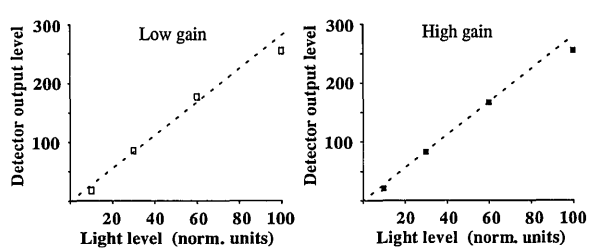

Fig. 2. Plots of the recorded signal as a function of detected light level for two different gains of the single MCP image intensifier. The light intensities used for the recordings with high gain were considerably lower than for the low-gain measurements.

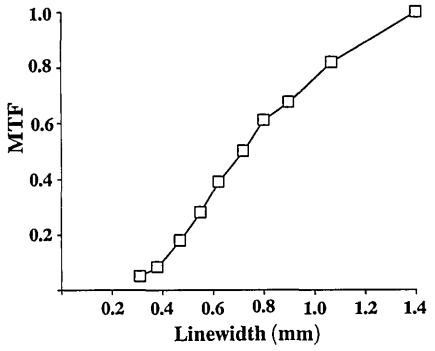

Fig. 3. Plot of the MTF of the system as a function of linewidth in a striped test object.

tion and detection efficiency of the system by dividing the images with images obtained from a cuvette filled with heavy fuel oil. An artificial image is produced by pixel-to-pixel calculations with the formula $F = [I(630) - k \times I(600)]/I(470)$, where k is a constant that corrects for the decrease in the tissue autofluorescence between 600 and 630 nm. In practice, the k factor also compensates for variations in detection sensitivity between the two wavelengths, which are judged by independent measurements. The processing yielded an artificial image in the dimensionless ratio between the background-free porphyrin signal and the tissue autofluorescence. In this image the demarcation of the tumor is clearly improved. The intensity from a cross section through the image is shown below each image. These intensity cross sections, which quantify the intensities for the same

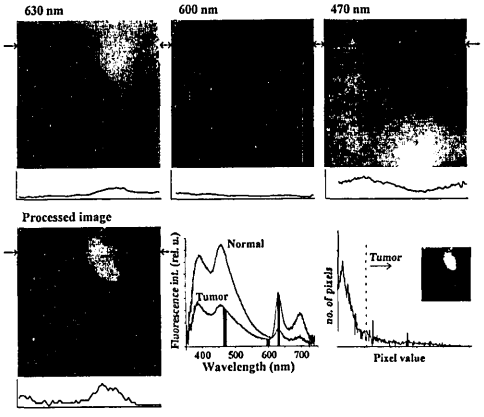

Fig. 4. Fluorescence images at 630, 600, and 470 nm, corrected for the spatial sensitivity variation in the system, are shown together with an image calculated pixel by pixel as $F = [I(630) - k \times I(600)]/I(470)$. The images show the same area (10 mm × 10 mm) of a rat muscle on the right hind leg. At 1:00 p.m. in the images a 1.5 mm × 3 mm tumor is present. The intensities in a cross section through the images are illustrated below each image. The fluorescence emission spectra from the tumor region and the surrounding muscle are shown as well. The last part of the figure shows a histogram, presenting the number of pixels with a certain function value in the processed image versus the function value. An insert of the processed image with all pixels below the indicated threshold represented as black and all above the same threshold as white is also shown. The data were accumulated for 50 readout following 337-nm excitation with the system with one MCP.

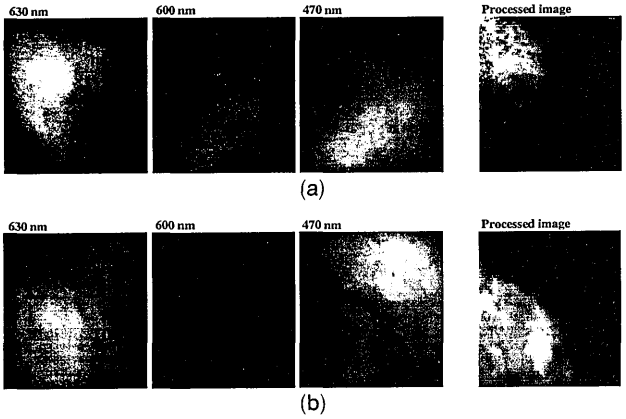

Fig. 5. Two examples of raw data and processed multicolor fluorescence images of tumors in rats, recorded under the same conditions as in Fig. 4, are shown. (a) Inoculated adenocarcinoma tumor growing in the hind leg muscle is shown in the upper-left corner of the images, (b) inoculated brain tumor is present in the lower-left corner of the images.

array of pixels in the various images, help in understanding the concept of the pixel-to-pixel calculation and the resultant processed image. They also show the improvement in tumor demarcation by the processing. In Fig. 4, the full fluorescence emission spectra, obtained with an optical multichannel-analyzer-based point fluorosensor, are illustrated for the tumor region and the surrounding muscle. The spectral differences between the tissue types, which form the basis for tissue identification in the multicolor fluorescence imaging system, are shown in the spectra. The filter profiles for the three filters used in this system are also indicated. In the last part of Fig. 4, a histogram of the pixel intensity in the processed image is given. In the histogram a peak can be seen at low processed function values. This peak reflects the many pixels from normal tissue with a low function value. A small number of pixels with higher function values can also be seen. These pixels do not form a second peak, but rather are smeared out over a wide range of function values. These high values indicate tumor tissue. A threshold function value for a tumor is indicated in the histogram. In the inset image all values below this threshold are coded as black and all pixels with higher values are represented with white. The tumor region is clearly visualized by this threshold.

In Fig. 5 two other typical examples of raw data and processed multicolor tumor images are presented. In Fig. 5(a) another image of an inoculated adenocarcinoma tumor in the hind leg of a rat is shown. The tumor is located in the upper-left corner in the images. The same set of images is shown in Fig. 5(b) for an RG-2 brain tumor. In these images the tumor is located in the lower-left corner. As can be seen, the tumor demarcation was clearly improved in both examples by the multicolor processing.

One example of multicolor imaging of an inoculated adenocarcinoma tumor by the use of the system with two MCP's is shown in Fig. 6. This set of images is

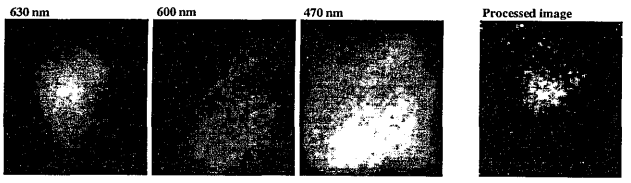

Fig. 6. Examples of images of an inoculated adenocarcinoma tumor in the muscle recorded with two MCP's at lower gain but otherwise under the same conditions as in Figs. 4 and 5. The tumor is located near the center of the images.

recorded with the same number of accumulations, but with a lower gain on each of the intensifiers compared with the recordings with only one MCP.

4. Discussion

Fluorescence has been shown to have a potential use in early tumor localization and identification. However, for fluorescence to become a widely accepted technique for routine clinical use, precise clinical applications have to be defined and investigated in detail. Also, improved equipment adapted for routine clinical use must be developed. The measurements presented here and elsewhere[17,18,20] suggest that the concept of multicolor fluorescence imaging certainly improves the potential for medical fluorescence diagnostics. The experience gained in the development of this preclinical system could be helpful in the construction of clinical systems. Especially the characteristics of the system in terms of sensitivity and image quality should be considered.

The lowest detectable signal is of interest for the sensitivity and dynamic range. The highest detectable signal is of further interest for quantifying the dynamic range. The highest signal that can be detected without saturation of the camera is the signal superimposed on a background signal, which corresponds to the maximum level of the standard CCIR video format. This signal in this system corresponded to just below the upper safe limit of exposure of the image intensifier in front of the CCD camera. The maximum current through the MCP therefore sets the upper limit of the signal level. The background signal, which consists of detected background light and detector dark current, will reduce the dynamic range of the detector in two ways: First, it will reduce the highest detectable signal, as it will add a subtractable offset level to the signal, and second it will add noise to the signal by means of the nonsubtractable uncertainty in the background signal. The lowest signal detectable is defined as a signal level equal to the root-mean-square noise.

At least five different types of noise source are of importance for such camera systems: photon noise, variation in intensifier gain, signal-induced noise, thermal noise, and readout noise. Photon noise is caused by the quantization of light and is due to statistical fluctuations in the signal radiation. Gain variations for individual photons are mainly due to statistical fluctuations in the number of electrons emitted in each step of intensification in the MCP image intensifier. In this respect, variations in the first steps in the intensification chain are of special importance, as these fluctuations will be amplified through all the following intensification steps. The effect of gain variations in a recorded image is most clearly seen for low light levels at high gains, for which detection of a small number of photons per pixel does not permit the noise to be averaged over many photons. Photon-counting sensitivity was easily reached when the system was used with two MCP's. The effect of gain variations could then be clearly seen, as each detected photon gave a different intensity. Signal-induced noise is caused by reflections and scattering within the image intensifiers. Its importance depends critically on the gain of the intensifiers. For high gains and low signal levels, it can be a noise source of importance. This effect causes a smoothing of sharp structures, especially for two MCP's. In comparing the image obtained with one MCP in Figs. 4 and 5 with the images of similar tissues obtained with 2 MCP's in Fig. 6, the limited dynamic range in the photon-counting mode (Fig. 6) is evident. The images in Fig. 6 are patchy in an incorrectable manner, and the patchness remains after processing. A reduced spatial resolution is also seen in Fig. 6, probably because of signal-induced noise. Thermal noise can cover several sources of noise, which leads to a non-signal-related charge buildup in the camera during the signal integration. This buildup is caused mainly by thermal generation of electron-hole pairs in the camera, but it is also to some extent caused by thermal emission of electrons from the photocathode of the image intensifier and by background radioactive radiation or radiation emitted from the camera housing. The uncertainty that is due to statistical variations in the number of quanta detected for both photon and thermal noise follow Poisson statistics. Readout noise is noise introduced in the electronics following the camera. This noise depends on the speed of the CCD readout but should be relatively independent of the signal level. Generally a slower readout speed will result in less noise added to the signal. The two latter noise sources had only minor influences on the data from this system. Apart from these noise sources, a truncation error will be introduced in the analog-to-digital converter.

The spatial resolution of the system will be the convolution of the resolution in the three main components: the optics, the image intensifier, and the CCD camera. The number of pixels in the CCD camera sets an upper limit for the spatial resolution. However, both the optics and the image intensifier will lower the resolution in the system presented. Aberrations in the optics reduce the image quality and its resolution. The aberrations depend on the numerical aperture and on the type and quality of the optical components. Scattering within the optical system will also reduce the image quality. An all-mirror optical system was chosen to permit independent adjustments of the four images and to eliminate

chromatic aberrations. This is of special importance in this system, as the four images at different wavelengths in the data evaluation will be compared on a pixel-to-pixel basis. The optics will limit the spatial resolution in this system if the full aperture of the system is used.

In the image intensifier the number of microchannels sets an upper limit for the resolution. Other limiting processes are electrons accelerated between the photocathode and the MCP and between the MCP and the phosphor, which may have a small velocity component perpendicular to the acceleration. This will smear the image. Furthermore, an electron hitting the phosphor will result in a finite size of the emitting spot. A reduction in spatial resolution will occur, especially at high gain, when electrons with a high velocity impinge on the phosphor.

The resolution in a system for tissue fluorescence in the red spectral region may not be critical, as the diffuse scattering within the tissue of red light with a relatively long penetration length will limit the red tissue fluorescence to low spatial frequencies. However, in a multicolor image processing system the diffuse scattering in tissue can become critical, as the different images will have different cutoff frequencies because of the variations of the optical properties at the various wavelengths. Such a system will thus not necessarily produce truly identical images of the object at different wavelengths. Such effects have been seen with the system, and this problem must be considered in the development of a clinical system. Tissue optics is also of importance for the probe depth of fluorescence diagnostics in tissue. The probe depth of the system is limited to a few hundred micrometers with the excitation wavelength used (337 nm). Only superficial lesions could thus be detected with this method. Still, this method can be used for a large number of clinical applications, as endoscopic techniques permit direct imaging of many early-stage tumors.

The use of a MCP image intensifier results in a system that is sensitive to low signals, which is of importance in avoiding too high light and tumor-marking drug doses in clinical applications. It also permits adequate suppression of any present background light because of the short gating period during the pulsed laser excitation. The gate width is short enough to allow the utilization of fluorescence decay characteristics of "late" fluorescence imaging to further improve the detection of tumor-marking drugs with long fluorescence lifetimes.[21,22] In some cases with low signal levels, for which two image intensifiers would be preferable, it might be better to use a diode intensifier in front of a MCP intensifier. A diode intensifier is a photocathode and a phosphor with a small gap with a high voltage in between. The gain in such an intensifier will be lower than that for a MCP, probably lower than a factor of 100. The secondary emission (i.e., the number of emitted electrons in the first intensification step) is better for a diode intensifier compared with a MCP, and thus the gain variation should be less pronounced when such an intensifier is used.

A drawback of using both two MCP's and a diode intensifier plus a MCP is that the suppression of background light is less efficient than for a single MCP. In many cases the detection limit is set by the signal-to-background rather than the signal-to-noise ratio. This is probably the case for endoscopies, in which the white-light illumination is bright.

A potential future system, adapted for routine clinical use, should probably apply a single MCP with as high a gain as possible. With such a system the best image quality is reached and still ambient background light can be suppressed efficiently. A clinical system should also be adapted to the optical-fiber bundle in an endoscope to permit endoscopic applications. The requirements of a clinical system in terms of speed are also critical. Fast processing is possible in a realistic computer. The limitation in the acquisition speed will probably be the light level for achieving high-quality images. Broader filters with higher transmissions will naturally replace the filters used here, once the repetition rate of the system is more critical. A more powerful light source might also be required. Based on the experience gained from the system presented in this paper, a clinically adapted, endoscopic system is now being implemented.

Discussions with Sune Montan and Katarina Svanberg are gratefully acknowledged, as is the support from the Lund University Medical Laser Centre. The work was supported by the Swedish Board for Technical Developments and by the Wallenberg Foundation and the Swedish Society for Cancer Research.

References

1. A. E. Profio, "Fluorescence diagnosis and dosimetry using porphyrins," in *Photodynamic Therapy of Neoplastic Tissue,* D. Kessel, ed. (CRC, Boca Raton, Fla., 1990), Vol. 1, pp. 77–89.
2. S. Andersson-Engels and B. C. Wilson, "In vivo fluorescence in clinical oncology: fundamental and practical issues," J. Cell. Pharmacol. **3,** 48–61 (1992).
3. S. Svanberg, "Tissue diagnostics using lasers," in *Lasers in Medicine,* G. Pettit and R. W. Waynant, eds. (Wiley, New York, to be published).
4. S. Andersson-Engels, J. Johansson, K. Svanberg, and S. Svanberg, "Fluorescence diagnostics and photochemical treatment of diseased tissue using lasers," Anal. Chem. **61,** 1367A–1373A (1989); Anal. Chem. **62,** 19A–27A (1990).
5. B. Chance, S. Nioka, J. Kent, K. McCully, M. Fountain, R. Greenfield, and G. Holtom, "Time resolved spectroscopy of hemoglobin and myoglobin in resting and ischemic muscle," Anal. Biochem. **174,** 698–707 (1988).
6. G. Müller, ed., *Medical Optical Tomography: Functional Imaging and Monitoring,* Vol. 11 of SPIE Institute Series (Society of Photo-Optical Instrumentation Engineers, Bellingham, Wash., 1993).
7. J. R. Lakowicz, *Principles of Fluorescence Spectroscopy* (Plenum, New York, 1983).
8. A. E. Profio, "Review of fluorescence diagnosis using porphyrins," in *Laser Surgery: Characterization and Therapeutics,* K. Atsumi and S. N. Joffe, eds., Proc. Soc. Photo-Opt. Instrum. Eng. **907,** 150–156 (1988).
9. A. E. Profio, O. J. Balchum, and F. Carstens, "Digital back-

ground subtraction for fluorescence imaging," Med. Phys. **13,** 717–721 (1986).
10. K. J. Brodbeck, A. E. Profio, T. Frewin, and O. J. Balchum, "A system for real time fluorescence imaging in color for tumor diagnosis," Med. Phys. **14,** 637–639 (1987).
11. G. Wagnières, Ch. Depeursinge, Ph. Monnier, M. Savary, P. Cornaz, A. Châtelain, and H. van den Bergh, "Photodetection of early cancer by laser induced fluorescence of a tumor-selective dye: apparatus design and realization," in *Photodynamic Therapy: Mechanisms II,* T. J. Dougherty, ed., Proc. Soc. Photo-Opt. Instrum. Eng. **1203,** 43–52 (1990).
12. E. Unsöld, R. Baumgartner, W. Beyer, D. Jocham, and H. Stepp, "Fluorescence detection and photodynamic treatment of photosensitized tumours in special consideration of urology," Lasers Med. Sci. **5,** 207–212 (1990).
13. B. Palcic, S. Lam, J. Hung, and C. MacAuley, "Detection and localization of early lung cancer by imaging techniques," Chest **99,** 742–743 (1991).
14. S. Andersson-Engels, J. Ankerst, S. Montán, K. Svanberg, and S. Svanberg, "Aspects of tumour demarcation in rats by means of laser-induced fluorescence and haematoporphyrin derivatives," Lasers Med. Sci. **3,** 239–248 (1988).
15. W. Lohmann and E. Paul, "Native fluorescence of unstained cryosections of the skin with melanomas and naevi," Naturwissenschaften **76,** 424–426 (1989).
16. S. Lam, C. MacAuley, J. Hung, J. LeRiche, A. E. Profio, and B. Palcic, "Detection of dysplasia and carcinoma *in situ* with a lung imaging fluorescence endoscopic device," J. Thorac. Cardiovas. Surg. **105,** 1035–1040 (1993).
17. S. Montán, K. Svanberg, and S. Svanberg, "Multi-color imaging and contrast enhancement in cancer-tumor localization using laser-induced fluorescence in hematoporphyrin-derivative-bearing tissue," Opt. Lett. **10,** 56–58 (1985).
18. P. S. Andersson, S. Montán, and S. Svanberg, "Multispectral system for medical fluorescence imaging," IEEE J. Quantum Electron. **QE-23,** 1798–1805 (1987).
19. S. Andersson-Engels, A. Brun, E. Kjellén, L. G. Salford, L.-G. Strömblad, K. Svanberg, and S. Svanberg, "Identification of brain tumours in rats using laser-induced fluorescence and haematoporphyrin derivative," Lasers Med. Sci. **4,** 241–249 (1989).
20. S. Andersson-Engels, J. Johansson, and S. Svanberg, "Multicolor fluorescence imaging system for tissue diagnostics," in *Bioimaging and Two-Dimensional Spectroscopy,* L. C. Smith, ed., Proc. Soc. Photo-Opt. Instrum. Eng. **1205,** 179–189 (1990).
21. S. Andersson-Engels, J. Johansson, U. Stenram, K. Svanberg and S. Svanberg, "Malignant tumor and atherosclerotic plaque diagnosis using laser-induced fluorescence," IEEE J. Quantum Electron. **26,** 2207–2217 (1990).
22. R. Cubeddu, G. Canti, P. Taroni, and G. Valentini, "Time-gated fluorescence imaging for the diagnosis of tumors in a murine model," Photochem. Photobiol. **57,** 480–485 (1993).